Under the hood of satellite empirical chlorophyll *a* algorithms: revealing the dependencies of maximum band ratio algorithms on inherent optical properties

Michael J. Sauer, [1,*] C. S. Roesler,[2] P. J. Werdell,[3] and A. Barnard[4]

[1]*US Geological Survey, 6000 J Street, Placer Hall, Sacramento, California 95819, USA*
[2]*Department of Earth and Oceanographic Science, Bowdoin College, Brunswick, Maine, 04011, USA*
[3]*NASA Goddard Space Flight Center, Code 616 Greenbelt, Maryland, 20771, USA*
[4]*Western Environmental Technology Laboratories Philomath, Oregon, 97370-0518, USA*
**msauer@usgs.gov*

Abstract: Empirically-based satellite estimates of chlorophyll *a* [Chl] (e.g. OC3) are an important indicator of phytoplankton biomass. To correctly interpret [Chl] variability, estimates must be accurate and sources of algorithm errors known. While the underlying assumptions of band ratio algorithms such as OC3 have been tacitly hypothesized (i.e. CDOM and phytoplankton absorption covary), the influence of component absorption and scattering on the shape of the algorithm and estimated [Chl] error has yet to be explicitly revealed. We utilized the NOMAD bio-optical data set to examine variations between satellite estimated [Chl] and in situ values. We partitioned the variability into (a) signal contamination and (b) natural phytoplankton variability (variability in chlorophyll-specific phytoplankton absorption). Not surprisingly, the OC3 best-fit curve resulted from a balance between these two different sources of variation confirming the bias by detrital absorption on global scale. Unlike previous descriptions of empirical [Chl] algorithms, our study (a) quantified the mean detrital:phytoplankton absorption as ~1:1in the global NOMAD data set, and (b) removed detrital (CDOM + non-algal particle) absorption in radiative transfer models directly showing that the scale of the remaining variability in the band ratio algorithm was dominated by phytoplankton absorption cross section.

OCIS codes: (280.4991) Passive remote sensing; (010.4450) Oceanic optics; (010.1690) Color; (010.1030) Absorption; (010.1350) Backscattering.

References and links

1. J. A. Yoder, "An overview of temporal and spatial patterns in satellite-derived chlorophyll-a imagery and their relation to ocean processes," in: *Satellites, Oceanography and Society* D. Halpern, ed. (Elsevier Oceanography Series, 2000), pp. 225–234.
2. W. W. Gregg, N. W. Casey, and C. R. McClain, "Recent trends in global ocean chlorophyll," Geophys. Res. Lett. **32**(3), L03606 (2005).
3. J. H. Ryther and D. W. Menzel, "Light adaptation by marine phytoplankton," Limnol. Oceanogr. **4**(4), 492–497 (1959).
4. P. G. Falkowski and T. G. Owens, "Light-shade adaptation: two strategies in marine phytoplankton," Plant Physiol. **66**(4), 592–595 (1980).
5. M. J. Perry, M. C. Talbot, and R. S. Alberte, "Photoadaptation in marine phytoplankton: response of the photosynthetic unit," Mar. Biol. **62**(2-3), 91–101 (1981).
6. L. N. M. Duyens, "The flattening of the absorption spectrum of suspensions, as compared to that of solutions," Biochim. Biophys. Acta **19**(1), 1–12 (1956).
7. J. T. O. Kirk, "A theoretical analysis of the contribution of algal cells to the attenuation of light within natural waters. I. general treatment of suspensions of pigmented cells," New Phytol. **75**(1), 11–20 (1975).

#163481 - $15.00 USD Received 22 Feb 2012; revised 11 Jul 2012; accepted 11 Jul 2012; published 29 Aug 2012

8. G. B. Mitchell and D. A. Kiefer, "Variability in pigment particulate fluorescence and absorption spectra in the northeastern Pacific Ocean," Deep-Sea Res. **35**(5), 665–689 (1988) (Part A).
9. N. P. Hoepffner and S. Sathyendrenath, "Bio-optical characteristics of coastal waters: Absorption spectra of phytoplankton and pigment distribution in the western North Atlantic," Limnol. Oceanogr. **37**(8), 1660–1679 (1992).
10. A. Bricaud, M. Babin, A. Morel, and H. Claustre, "Variability in the chlorophyll-specific absorption coefficients of natural phytoplankton: analysis and parameterization," J. Geophys. Res. **100**(C7), 13321–13332 (1995).
11. D. A. Siegel, S. Maritorena, N. B. Nelson, M. J. Behrenfeld, and C. R. McClain, "Colored dissolved organic matter and its influence on the satellite-based characterization of the ocean biosphere," Geophys. Res. Lett. **32**(20), L20605 (2005).
12. D. A. Siegel, S. Maritorena, N. B. Nelson, and M. J. Behrenfeld, "Independence and interdependencies among global ocean color properties: Reassessing the bio-optical assumption," J. Geophys. Res. **110**(C7), C07011 (2005).
13. A. Morel and B. Gentili, "A simple band ratio technique to quantify the colored dissolved and detrital organic material from ocean color remotely sensed data," Remote Sens. Environ. **113**(5), 998–1011 (2009).
14. H. Loisel, B. Lubac, D. Dessailly, L. Duforet-Gaurier, and V. Vantrepotte, "Effect of inherent optical properties variability on the chlorophyll retrieval from ocean color remote sensing: an in situ approach," Opt. Express **18**(20), 20949–20959 (2010).
15. M. Szeto, P. J. Werdell, T. S. Moore, and J. W. Campbell, "Are the world's oceans optically different?" J. Geophys. Res. **116**, C00H04 (2011).
16. H. R. Gordon, O. B. Brown, R. H. Evans, J. W. Brown, R. C. Smith, K. S. Baker, and D. K. Clark, "A semiananalytic radiance model of ocean colour," J. Geophys. Res. **93**, 10,909–10,924 (1988).
17. A. Morel, "Optical modeling of upper ocean in relation to its biogenous matter content (Case 1 waters)," J. Geophys. Res. **93**(C9), 10,749–10,768 (1988).
18. O. Ulloa, S. Sathyendranath, and T. Platt, "Effect of the particle-size distribution on the backscattering ratio in seawater," Appl. Opt. **33**(30), 7070–7077 (1994).
19. IOCCG, "Remote sensing of ocean color in coastal, and other optically-complex waters," in *Reports of the International Ocean-Colour Coordinating Group, No. 3* Sathyendranath, S. (ed.), (IOCCG, 2000), p. 140.
20. H. R. Gordon and A. Morel, "Remote assessment of ocean color for interpretation of satellite visible imagery: a review," *Lecture Notes on Coastal and Estuarine Studies, Volume 4* (Springer-Verlag, 1983).
21. A. Morel and L. Prieur, "Analysis of variations in ocean color," Limnol. Oceanogr. **22**(4), 709–722 (1977).
22. C. A. Brown, Y. Huot, P. J. Werdell, B. Gentili, and H. Claustre, "The origin and global distribution of second order variability in satellite ocean color and its potential application to algorithm development," Remote Sens. Environ. **112**(12), 4186–4203 (2008).
23. S. B. Hooker, C. R. McClain, J. K. Firestone, T. L. Westphal, E. N. Yeh, and Y. Geo, "The SeaWiFS Bio-optical Archive and Storage System (SeaBASS), part 1.," NASA Tech. Memo., 104566, Vol. 20, (Greenbelt: NASA Goddard Space Flight Center, 1994), p. 37.
24. NASA, "SEABASS", http://seabass.gsfc.nasa.gov/
25. S. C. Alvain, C. Moulin, Y. Dandonneau, and F. M. Bréon, "Remote sensing of phytoplankton groups in case 1 waters from global SeaWiFS imagery," Deep-Sea Res. **92**, 14411–14415 (2005).
26. S. C. Alvain, C. Moulin, Y. Dandonneau, H. Loisel, and F. M. Breon, "A species dependent bio-optical model of case I waters for global ocean color processing," Deep Sea Res. Part I Oceanogr. Res. Pap. **53**(5), 917–925 (2006).
27. . Alvain, C. Moulin, Y. Dandonneau, and H. Loisel, "Seasonal distribution and succession of dominant phytoplankton groups in the global ocean: A satellite view," Global Biogeochem. Cycles **22**(3), GB3001 (2008), doi:10.1029/2007GB003154.
28. R. A. Barnes, D. K. Clark, W. E. Esaias, G. S. Fargion, G. C. Feldman, and C. R. Mcclain, "Development of a consistent multi-sensor global ocean colour time series," Int. J. Remote Sens. **24**(20), 4047–4064 (2003).
29. G. S. Fargion and C. R. McClain, SIMBIOS project 2003 annual report, NASA Tech. Memo., 2003–212251, (Greenbelt: NASA Goddard Space Flight Center, 2003), 202.
30. C. R. McClain, W. Esaias, G. Feldman, R. Frouin, W. Gregg, and S. B. Hooker, "The proposal for the NASA Sensor Intercalibration and Merger for Biological and Interdisciplinary Oceanic Studies (SIMBIOS) Program, NASA Tech. Memo. 2002-210008, (Greenbelt: NASA Goddard Space Flight Center, 2002), 65.
31. P. J. Werdell, "An evaluation of inherent optical property data for inclusion in the NASA bio-Optical Marine Algorithm Data set," NASA Ocean Biology Processing Group, Science Systems and Applications, Inc. Document Version 1.1, corresponding to NOMAD Version 1.3, (2005).
32. P. J. Werdell and S. W. Bailey, "An improved in-situ bio-optical data set for ocean color algorithm development and satellite data product validation," Remote Sens. Environ. **98**(1), 122–140 (2005).
33. S. A. Garver and D. A. Siegel, "Inherent optical property inversion of ocean color spectra and its biogeochemical interpretation. 1. time series from the Sargasso Sea." J. of Geophys. Res.- Oceans **102**(C8), 18607–18625 (1997).
34. S. Maritorena, D. A. Siegel, and A. R. Peterson, "Optimization of a semianalytical ocean color model for global-scale applications," Appl. Opt. **41**(15), 2705–2714 (2002).
35. K. Baith, R. Lindsey, G. Fu, and C. R. McClain, "SeaDAS: a data analysis system for ocean color satellite sensors," in *EOS, Trans. Am. Geophys. Union*, (2000).

#163481 - $15.00 USD Received 22 Feb 2012; revised 11 Jul 2012; accepted 11 Jul 2012; published 29 Aug 2012

36. R. M. Pope and E. S. Fry, "Absorption spectrum (380-700 nm) of pure water. II. Integrating cavity measurements," Appl. Opt. **36**(33), 8710–8723 (1997).
37. A. Morel, "Optical properties of pure seawater," In: *Optical Aspects of Oceanography* N. G. Jerlov and E. Steemann Nielsen, eds. (Academic Press Inc., 1974), pp. 1–24.
38. H. R. Gordon, O. B. Brown, and M. M. Jacobs, "Computed relationships between the inherent and apparent optical properties of a flat homogeneous ocean," Appl. Opt. **14**(2), 417–427 (1975).
39. Z. P. Lee, K. L. Carder, C. D. Mobley, R. G. Steward, and J. S. Patch, "Hyperspectral remote sensing for shallow waters. 2. Deriving bottom depths and water properties by optimization," Appl. Opt. **38**(18), 3831–3843 (1999).
40. A. Bricaud, A. Morel, M. Babin, K. Allali, and H. Claustre, " Variations of light absorption by suspended particles with chlorophyll *a* concentration in oceanic (case 1) waters: analysis and implications for bio-optical models, " J. Geophys. Res. **103**(C13), 31033–31044 (1998).
41. H. Loisel and A. Morel, "Light scattering and chlorophyll concentration in case 1 waters: a re-examination," Limnol. Oceanogr. **43**(5), 847–858 (1998).
42. A. Morel, D. Antoine, and B. Gentili, "Bidirectional reflectance of oceanic waters: accounting for Raman emission and varying particle scattering phase function," Appl. Opt. **41**(30), 6289–6306 (2002).
43. J. T. O. Kirk, "Dependence of relationship between inherent and apparent optical properties of water on solar altitude," Limnol. Oceanogr. **29**(2), 350–356 (1984).
44. J. E. O'Reilly, S. Maritorena, B. G. Mitchell, D. A. Siegel, K. L. Carder, S. A. Garver, M. Kahru, and C. R. McClain, "Ocean color chlorophyll algorithms for SeaWiFS," J. Geophys. Res. **103**(C11), 24937–24953 (1998).
45. P. Legendre and L. Legendre, *Numerical Ecology*, 2nd English ed. (Elsevier Science BV, 1998), p. 853.
46. M. Babin, A. Morel, V. Fournier-Sicre, F. Fell, and D. Stramski, "Light scattering properties of marine particles in coastal and open ocean waters as related to the particle mass concentration," Limnol. Oceanogr. **48**(2), 843–859 (2003).
47. G. E. Fogg and G. T. Boalch, "Extracellular products in pure cultures of a brown alga," Nature **181**(4611), 789–790 (1958).
48. C. S. Yentsch and C. A. Reichert, "The interrelationship between water soluble yellow substances and chloroplastic pigments in marine algae," Bot. Mar. **3**, 65–74 (1961).
49. H. Sasaki, T. Miyamura, S. Saitoh, and J. Ishizaka, "Seasonal variation of absorption by particles and colored dissolved organic matter (CDOM) in Funka Bay, southwestern Hokkaido, Japan," Estuar. Coast. Shelf Sci. **64**(2-3), 447–458 (2005).

1. Introduction

Over the last 30 years, a major focus of the interpretation of ocean color has been estimating the surface concentration of chlorophyll *a,* the major light absorbing pigment in phytoplankton and proxy for phytoplankton biomass. Synoptic empirically-based satellite estimates of chlorophyll *a* concentration (mg m^{-3}; [Chl]), such as those obtained with the sequencing maximum band ratio algorithms OC3 (MODIS) and OC4 (SeaWiFS), provide important indicators of the condition of marine ecosystems. The ubiquitous use of empirical satellite [Chl] estimates and their importance as a phytoplankton biomass index [1,2] despite confounding issues of photadaptation [3–5] dictates that the estimates must be accurate and that knowledge of the errors and biases are necessary in order to correctly interpret [Chl] variability. This is all the more important given the inclusion of empirical satellite [Chl] estimates in the NASA Earth System Data Record.

The task of estimating [Chl] from remotely-sensed ocean color has been considerably difficult at regional and local scales because the spectral inherent optical properties (IOPs) of the ocean influencing the color of the ocean are both diverse and complex. Major sources of variation in the bulk IOP signals are due to the quantity and spectral quality of dissolved and particulate material which are a function of the variability in phytoplankton community composition, inorganic suspended particles, chromophoric dissolved organic material (CDOM), and non-algal particles (NAP). The shape of the chlorophyll *a*-specific phytoplankton absorption spectrum (m^2 mg chl^{-1}; a_{ph}^* (λ)) has been shown to be widely variable, dependent on pigment complement ([Chl] + accessory pigments), pigment packaging, physiological state of the cell, and community composition [6–10]. Detrital absorption, characterized by a wavelength dependent exponentially decreasing spectrum, are often defined as the combination of CDOM, NAP and inorganic particles. Both inorganic particle and detrital absorption have been found to be non-covarying factors in the open ocean [11,12]. The lack of covariance between bio-optical components and their common strong

#163481 - $15.00 USD Received 22 Feb 2012; revised 11 Jul 2012; accepted 11 Jul 2012; published 29 Aug 2012

absorption of blue and blue-green light are confounding influences on empirical satellite [Chl] estimates [11–15].

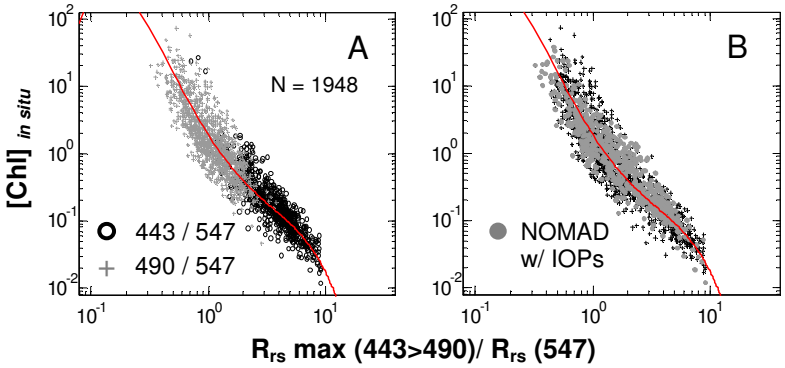

Fig. 1. MODIS OC3 4th degree polynomial algorithm (red line) overlaid on the maximum reflectance band ratios. A) OC3 (MBR; 443/547nm: black circles; 490/547nm: gray +) relationship with *in situ* [Chl] from the NOMAD data set. B) NOMAD *in situ* data set of [Chl] vs. MBRs (+) with coincident IOP data set.

The magnitude of the upwelling light field measured in remotely sensed applications is dominated by light scattered in the backward directions. Backscattering has been shown to globally covary with [Chl] in the surface waters, although the variations in the global relationship are large [16–18]. Spectral particle backscattering (m^{-1}; b_{bp}) has minimal wavelength dependence relative to absorption and is characterized by a slope of λ^{-n} where n varies from 0 to 2 suggesting that the spectral slope of backscattering plays a minor, secondary role in determining the spectral variability of global ocean color [19].

Ocean color varies approximately with backscattering and inversely with absorption [20,21], which globally, depends primarily on phytoplankton community structure. Since chlorophyll *a* is the main phytoplankton absorbing pigment, ocean color is indirectly dependent on [Chl] to first order such that as the ocean shifts from oligotrophic (low [Chl]) to eutrophic water (high [Chl]), a gradient of blue to blue-green color is traversed [21]. Empirical algorithms exploit this absorption dependency, statistically linking changing remotely-sensed reflectances (sr^{-1}; $R_{rs}(\lambda)$) with the gradient in [Chl]. For example, the OC3 (Fig. 1) empirical [Chl] algorithm use maximum band ratios (MBRs) of blue to blue-green (443 or 490nm) wavelengths, where phytoplankton absorption is strong, to green (547nm) wavelengths where phytoplankton absorption is relatively weak. Because phytoplankton and detrital matter absorption overlap in the blue to blue-green, however, MBRs do not carry unique information about [Chl].

As such, the success of empirical algorithms rests on the global mean covariation of phytoplankton with detrital absorption and particulate backscattering. This indicates that errors in the estimates of [Chl] may occur wherever and whenever the standard of component absorption covariation is not met [14,15]. Consequently, [Chl] empirical algorithms approach only 35% accuracy in Case 1 water and may be worse in Case 2 waters [19]. This disagreement with the 'bio-optical covariation assumption' was thought to only occur only in Case 2 waters where optical constituents vary independently. However, the lack of covariation has been shown in many different Case 1 ocean environments [11–15], suggesting that the well-recognized variability feature of empirical algorithms relates to cases where second order variability exists.

Clearly, satellite empirical [Chl] algorithms are complicated in their IOP dependencies. The details of the foundation of the [Chl] empirical algorithms have been tacitly hypothesized (i.e CDOM absorption covaries with phytoplankton), and the dispersion patterns within the

#163481 - $15.00 USD Received 22 Feb 2012; revised 11 Jul 2012; accepted 11 Jul 2012; published 29 Aug 2012

algorithm training sets have explicitly revealed with respect to the role of detrital and phytoplankton absorption or particulate backscattering [14,15,17–19,22]. However, previous work has provided only confirmation of existing biases (sometimes with conflicting proposed mechanisms for these biases) or relied on extensive modeling. Using the NASA bio-Optical Marine Algorithm Data set (NOMAD) [23,24], Brown et al. [22] found the impact of b_{bp} spectral slope, n, on the OC4 MBR algorithm to be ten times less than $b_{bp}(\lambda)$ and $a_{dm}(\lambda)$. Brown et al. [22] also suggested that the anomaly patterns in the MBR-[Chl] polynomial regression were related to differences in particulate backscattering rather than phytoplankton absorption. This is contrary to previous results attributing the anomaly patterns in b_{bp} to functional group differences in Alvain et al. [25–27]. More recently, Loisel et al. [14] and Szeto et al. [15] confirmed the well-known detrital absorption bias in OC3 or OC4 and its impact on [Chl] retrievals. However, both of these studies stop short of quantifying the covariance structure of phytoplankton and detrital absorption, or the impact of a_{ph}^* and b_{bp} probability on the shape of OC3 or OC4.

In this study, we confirm and quantify the impacts of the component absorption bias. We expand the analysis by looking under the hood of the MODIS OC3 empirical [Chl] algorithm and exploring the relationships between remote-sensing MBRs, in situ [Chl], and the discrete IOP measurements found in the in situ NOMAD training data set used to develop the bio-optical algorithm. First, we provide an IOP perspective of the OC3 empirical model similar to previous studies [13–15] but with attention to defining and quantifying the extent of the correlation between phytoplankton absorption and detrital absorption. Second, we further explore the basis of the algorithm by examining the global variability of a_{ph}^* that underlies the OC3 empirical model after removal of the detrital absorption component. Third, we test the sensitivity of MBR empirical models to variability in a_{ph}^* and backscattering probability through radiative transfer simulations. These extra steps go beyond recognizing the pattern of impact that detrital absorption has on empirical algorithms by observing and quantifying the impact of each component separately on the structure of the empirical algorithm.

2. Methods

Our approach is divided into three sections: (1) analysis of component absorption and backscattering within the NOMAD data set where the interrelationship between IOPs are both confirmed and quantified, (2) development of a detrital absorption free radiative transfer model derived from NOMAD in situ data for exposing how detrital absorption influences the curvature of OC3 and for determining the range of variability leftover in the model without detrital influence, and (3) development of a Hydrolight model of reflectances based on models of a_{ph}^* and $\tilde{b}_{bp}$ to isolate the influence of phytoplankton absorption and particle size on empirical algorithms. The overarching analysis is focused on identifying trends that affect global retrieval of [Chl] and are inherent in the NOMAD data set. While previous work has explored (1) [14,15,17–19,22], to our knowledge, analyses such as (2) and (3) have yet to be executed.

2.1. NOMAD in situ Data set – Component Relationships

The NOMAD data set was compiled using the NASA SeaWiFS Bio-optical Archive and Storage System (SeaBASS) [23,24] and was developed as part of the NASA Sensor Intercomparison and Merger of Biological and Interdisciplinary Ocean Studies (SIMBIOS) Program [28–30] for supporting present and future satellite ocean color missions. The data set includes both open ocean and coastal data sets [31,32].

The global bio-optical data set used in this study is a subset of NOMAD that includes in situ measured above water remote sensing reflectance and a set of matching depth-weighted discrete samples (n = 771) of coincident phytoplankton absorption and detrital absorption (CDOM + NAP) plus particulate backscattering (n = 331) (for information on database quality control, depth-weighting, and processing see [31,32]). This subset of NOMAD also includes

#163481 - $15.00 USD Received 22 Feb 2012; revised 11 Jul 2012; accepted 11 Jul 2012; published 29 Aug 2012

co-located and depth-weighted measurements of [Chl]. These measurements were a combination of HPLC [Chl] (primary) and fluorometric [Chl] (secondary). Component (phytoplankton and detrital (CDOM + NAP)) absorption was compared with [Chl] and between each component to determine relative variability and covariation in the NOMAD data set.

Because original b_{bp} measurements were limited in quantity (n = 331) and geographic distribution relative to absorption measurements (n = 771), sample numbers of b_{bp} were augmented to match sample numbers of in situ absorption measurements. We used the Garver-Siegel-Maritorena (GSM) semi-analytic algorithm [33,34] to estimate $b_{bp}(\lambda)$ (Table 4.2) employing standard coefficients set from the SeaWiFS Data Analysis System [SeaDAS; 35]. Realizing that the use of modeled data could introduce biases into our analyses, we confirmed that the GSM modeled b_{bp} at 443, 489, and 547nm matched closely to *in situ* measured values (443nm, slope (s.d). = 1.06 (0.03); 489nm, slope = 1.05 (0.03); 547nm, 1.03 (0.03). We further verified that biases were not introduced by GSM modeling of $b_{bp}(\lambda)$ by confirming the dynamic ranges of the in situ and modeled data sets aligned (data not shown).

2.2 Forward Model of Detrital Absorption Free Reflectance

Reflectance spectra, from which the contribution by detrital matter absorption was removed, were calculated from the remaining NOMAD IOPs in the following manner. Phytoplankton absorption measurements from the NOMAD data set and particulate backscatter measurements derived from NOMAD and GSM retrievals were combined with spectral water absorption [36] and backscatter measurements of water [37] at MODIS wavelengths (443, 490, 547nm) in a forward model. All particles were assumed to be of phytoplankton origin. Detrital (CDOM + NAP) absorption-free reflectances (a_{dm}-free) were then derived according to Gordon et al. [38] and Morel and Prieur [21]:

$$u(\lambda) = [b_{bw}(\lambda) + b_{bp}(\lambda)] / [a_w(\lambda) + a_{ph}(\lambda) + b_{bw}(\lambda) + b_{bp}(\lambda)]; \quad (1)$$

$$r_{rs}(0-, \lambda, sr^{-1}) = g_0 u(\lambda) + g_1 u(\lambda)^2; \quad (2)$$

where $g_0 = 0.0949$, $g_1 = 0.0794$, and $r_{rs}(0-, \lambda)$ indicates the remote-sensing reflectance just below the air-seawater interface.

Below water remote-sensing reflectance was transferred across the seawater interface following Lee et al. [39]:

$$R_{rs}(0+, \lambda, sr^{-1}) = 0.52 r_{rs}(\lambda) / [1 - 1.7 r_{rs}(\lambda)] \quad (3)$$

Similar to the OC3 algorithm, a fourth order modified polynomial fit (OC3") was applied to the a_{ph} and b_{bp} dependent [Chl] to MBR relationship:

$$log10[Chl] = a_1 + a_2 log_{10}(r) + a_3 log_{10}(r) + a_4 log_{10}(r) + a_5 log_{10}(r) \quad (4)$$

where (r) corresponds to the blue-green MBR defined as:

$$r = max\left(R_{rs}(443) > R_{rs}(490)\right) / R_{rs}(547) \quad (5)$$

2.3 Radiative Transfer Model Computations of Detrital Absorption – Free Reflectance

The radiative transfer model software package Hydrolight was used to compute above-water reflectances from a vertically homogeneous water column for a series of [Chl] (0.005-50 mg m^{-3}), in an infinitely deep water column during clear sky, low wind (5 m/s), and annual averaged sunlight conditions. Each set of [Chl] model runs included a series of a_{ph}* (0.11, 0.050, 0.022, 0.018 m^2 mg chl^{-1} at 444nm) computed from the power law model of Bricaud et al. [10,40] and corresponding to [Chl] (0.005-10mg m^{-3}). Contributions of detrital (CDOM,

#163481 - $15.00 USD Received 22 Feb 2012; revised 11 Jul 2012; accepted 11 Jul 2012; published 29 Aug 2012

NAP) and inorganic particles were not added to the absorption model such that above-water radiative transfer modeled reflectances were dependent only on absorption and scattering by water and phytoplankton.

Spectral scattering was derived from the difference of attenuation and absorption where attenuation was modeled based on [Chl] following the near-surface model developed by Loisel and Morel [41; their Eq. (5)]:

$$c_p(z,\lambda) = c_0\left[Chl\right](z)^n\ (\lambda/660)^v \tag{6}$$

where $c_0 = 0.407$, $n = 0.795$ and v is a function of [Chl],

$$\begin{aligned} v &= 0.5\left[log_{10}Chl - 0.3\right], && \text{for } 0 < \left[\text{Chl}\right] < 0.2 \\ v &= 0, && \text{for } \left[\text{Chl}\right] > 0.2 \end{aligned} \tag{7}$$

Backscattering probability, $\tilde{b}_{bp}$, was parameterized based on Morel et al. [42] Case 1 Small/Large particle scattering phase functions constituting backscatter proportions of 1.40% and 0.19% respectively. This corresponded to particle sizes ranging from 0.02 to 14μm (diameter of equivalent sphere with equal geometric cross-section) for phytoplankton-like particles with a refractive index of 1.06. Additionally, all model runs were made incorporating Raman scattering.

Each model computation in Hydrolight was preset to be run to a depth of at least $2/K_d$ (min) to ensure the capture of all photons influencing the surface ocean color, where K_d (min) is the minimum value of $K_d(\lambda)$ estimated following Kirk [43]:

$$K_d(\lambda) = [a_T(\lambda)^2 + 0.256 a_T(\lambda) b_T(\lambda)]^{0.5} \tag{8}$$

where

$$a_T(\lambda) = a_w(\lambda) + \left[Chl\right] a^*_{ph}(\lambda); \qquad [10] \tag{9}$$

$$b_T(\lambda) = b_w(\lambda) + 0.3\left[Chl\right]^{0.62}(550/\lambda) \qquad [20] \tag{10}$$

2.3 Statistical Evaluation

Slopes and intercepts of the regressions between OC3 estimated and in situ [Chl] as well as between IOP components were based on log-transformed data. This transformation is necessary because [Chl] has been shown to be more normally distributed when transformed [44] and the dynamic range of the biogeochemical variables is large. Analyses were made using Type II (major axis) regressions because sampling and systematic errors were present in both abscissa and ordinate variables and each paired variables were of the same unit and scale [45].

3. Results and Discussion

3.1 IOP Relationships within the OC3 Algorithm

Phytoplankton absorption in the in situ NOMAD subset exhibited a stronger least-squares power law relationship with [Chl] at 443 and 489nm than did detrital absorption (Fig. 2). Dispersion in a_{dm} around the best fit line relationship with [Chl] was ~2 orders of magnitude compared to ~1 for a_{ph}. In both a_{ph} and a_{dm}, the range of dispersion was mostly conserved throughout the range in [Chl]. Log-transformed phytoplankton and detrital absorption at 443 and 489nm were significantly correlated ($r = 0.78$ at 443nm; $r = 0.76$ at 489nm; $p<0.001$ for both) with similar slopes at different wavelengths (Fig. 3). The distribution of a_{dm} vs. [Chl] (Fig. 2) indicates that variability in a_{dm} was the primary source of dispersion in the a_{ph}:a_{dm}

#163481 - $15.00 USD Received 22 Feb 2012; revised 11 Jul 2012; accepted 11 Jul 2012; published 29 Aug 2012

relationship at both 443 and 489nm. Variability in the a_{ph}:a_{dm} relationship was limited at high a_{ph} (e.g high [Chl]) as the number of observations with relatively high a_{ph} with low a_{dm} was not present in the NOMAD data set at either wavelength. In contrast, at low a_{ph}, relatively high and low a_{dm} were both found. This suggests that non-covariance in the NOMAD data set was most likely to occur at low [Chl] where the dynamic range of a_{dm} was greatest.

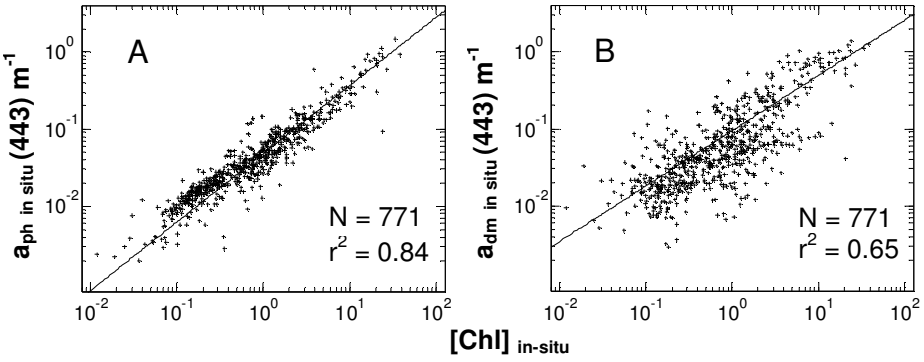

Fig. 2. NOMAD in situ a_{ph} (443) (A) and a_{dm} (443)(B) vs. in situ [Chl]. Line indicates power law relationship with [Chl] of the form Ax^B. In situ a_{ph} (489) and a_{dm} (489) (not shown) were similarly dispersed in their relationship with [Chl].

Higher amplitudes of b_{bp} were associated with increased levels of phytoplankton and detrital absorption. However, with respect to [Chl], highest amplitudes of b_{bp} were associated with a_{ph}:a_{dm} ratios that were <1 (Fig. 3) suggesting that non-algal particles and detrital material play a large role in high backscattering, high [Chl] waters. An independent analysis of component IOP contributions by Babin et al. [46] in European waters also show a similar dependence of a_{dm}, where the upper range of [Chl] was associated with an a_{dm} signal dominated by NAP. This is consistent with post-phytoplankton bloom samples where non-algal particles increased after peak phytoplankton biomass had been reached [47–49]. Once the component IOP relationships are displayed against the OC3 model curve, the absorption bias in the empirical [Chl] model becomes evident (Fig. 4). Above the OC3 model line, a_{ph} is the dominant absorption signal (a_{ph}:a_{dm}>1), while a_{dm} dominates below the best fit line (where a_{ph}:a_{dm}<1). At the ends of the data distribution, the lowest [Chl] are dominated by a_{dm} and very low b_{bp} while the highest in situ [Chl] is dominated by a_{ph}. Similar to Fig. 2, at high [Chl], high b_{bp} values are found dominating the region below the OC3 model line for very low MBRs.

#163481 - $15.00 USD Received 22 Feb 2012; revised 11 Jul 2012; accepted 11 Jul 2012; published 29 Aug 2012

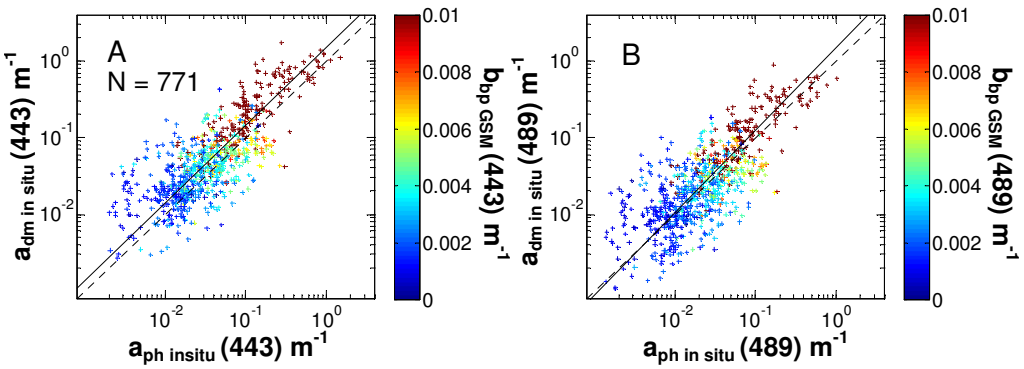

Fig. 3. Covariance of detrital and phytoplankton absorption. Covariation between NOMAD in situ a_{ph} and a_{dm} at 443nm (A) and 489nm (B), color coded by the magnitude of b_{bp} (443) or b_{bp} (489) from GSM retrievals. Dashed lines are 1:1. See Table 2 for regression results.

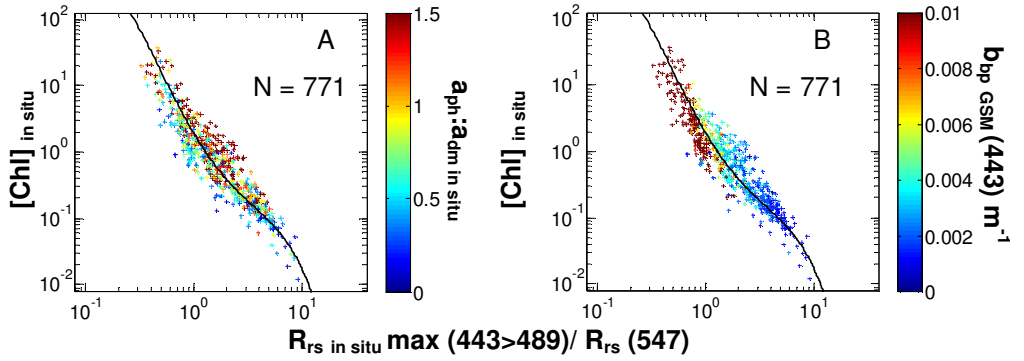

Fig. 4. IOP variability in the OC3 algorithm. NOMAD in situ [Chl a] vs. MBRs. Coincident samples are colored by a_{ph}:a_{dm} (A) at 443 or 490 determined by max MBR wavelength or (B) b_{bp}(443). Solid line indicates OC3.

Removal of detrital absorption (a_{dm}-free) from the reflectance signal revealed a 4th degree polynomial (OC3") that was a better fit (see Table 1) to [Chl] (Fig. 5) than OC3 (Fig. 4). The new relationship between MBRs and [Chl] was independent of a_{ph}:a_{dm} ratio suggesting that component absorption bias was removed in the OC3" empirical model. The correlation between b_{bp} and [Chl], however, remained in the empirical model relationship.

#163481 - $15.00 USD Received 22 Feb 2012; revised 11 Jul 2012; accepted 11 Jul 2012; published 29 Aug 2012

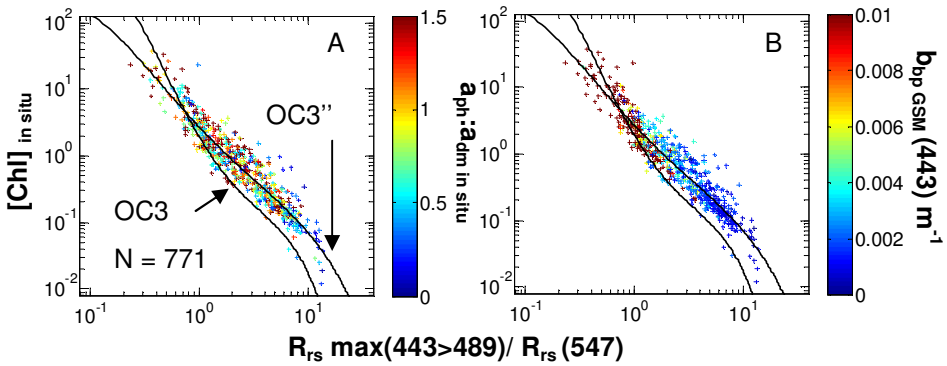

Fig. 5. The detrital-free OC3" colored by in situ a_{ph}:a_{dm} at 443 or 490 determined by maximum MBR wavelength (A) and b_{bp} (B, 443nm). The OC3 model fit is provided for comparison.

3.2 Empirically estimated [Chl] vs. in situ [Chl]

OC3 is a two-wavelength (max 443>490nm) switching MBR algorithm with different [Chl]-estimate statistical performance when evaluated individually by wavelength used in the MBR rather than as a pooled population (see Fig. 1; Table 1). Overall, the algorithm performs best (slope is ~1) when estimating [Chl] over a broad range of MBR values including data sets from both wavelength ratios. The overall pooled statistical success, however, disguises its relative shortcomings in oligotrophic 'blue' ocean conditions, below [Chl] of ~0.5-1.0 mg m^{-3}, when the algorithm switches to 443/547 rather than 490/547. The differences in the regression slopes between the two MBRs imply that the underlying IOP relationships of absorption and scattering with [Chl] and ocean color are presumably different along the gradient in the model.

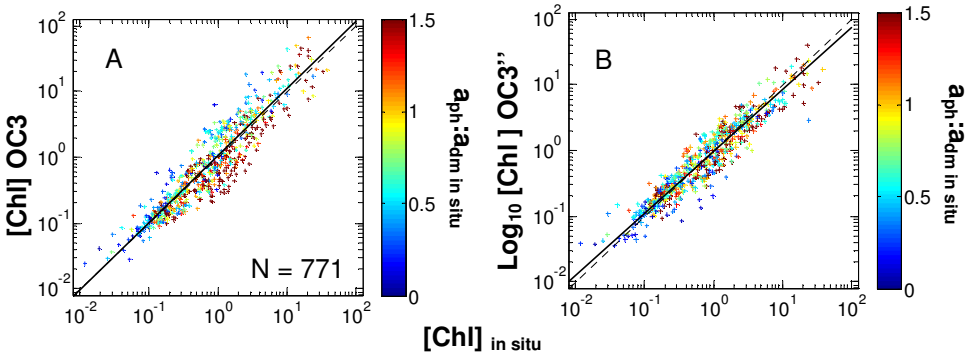

Fig. 6. OC3 (A) and OC3" (B) retrieved Chl a vs. in situ [Chl]. Data points are colored by in situ a_{ph}:a_{dm} at 443 or 490 determined by max MBR wavelength. Dashed lines are 1:1.

There was a clear component absorption based bias in the distribution of estimated [Chl] from OC3 (Fig. 6(A); Table 1; r^2 = 0.85 for full NOMAD or IOP subset) while the relationship between OC3" estimated [Chl] and in situ [Chl] was tighter with little or no component absorption bias (Fig. 6(B); Table 1; r^2 = 0.88). High a_{ph}:a_{dm} was associated with underestimated [Chl] and low a_{ph}:a_{dm} with overestimated [Chl]. This was an expected result because OC3 inherently assumes some covariation between a_{ph} and a_{dm}. Consequently, when there is relatively very low a_{dm}, OC3 attributes a portion of the reflectance signal to a_{dm} rather

#163481 - $15.00 USD Received 22 Feb 2012; revised 11 Jul 2012; accepted 11 Jul 2012; published 29 Aug 2012

than a_{ph}, and [Chl] is underestimated. Similarly, when more a_{dm} is present than expected OC3 overestimates [Chl] by assuming some of the a_{dm} signal is due to a_{ph}.

Low b_{bp} waters (in situ [Chl] range from 0.01 to ~5 mg m^{-3}) underestimated [Chl], while high b_{bp} waters ([Chl] range ~0.1 to 20 mg m^{-3}) generally overestimated [Chl]. Under or overestimates corresponding to b_{bp} amplitude and low or high [Chl] suggest that the spectral slope of b_{bp} drives these biases. Where [Chl] is low and b_{bp} slope increasingly negative, reflectance at 443nm is increased relative to 547nm driving the color of the ocean towards shorter wavelengths and lower estimated [Chl] than expected from a global mean spectral b_{bp}. For higher [Chl], the opposite is expected, as b_{bp} at 547nm is increased relative to 443 or 490nm, b_{bp} spectral slope is flattened, and MBR is reduced driving the ocean toward a green color. While it appears that spectral slope does exert an influence on the shape of OC3 and [Chl] errors, the Brown et al. [22] model analysis of MBR anomalies based on b_{bp} spectral slope suggests that it is relatively minor influence.

Table 1. Estimated [Chl] performance statistics. Slope and intercept statistics with (standard deviation) for the comparison of OC3 and OC3" [Chl] estimates with in situ [Chl] defined by MBR utilized: 443/547 (~low [Chl]), 490/547 (~high [Chl]), or overall results. For OC3 (full NOMAD), N = 1984; for OC3 (IOP subset) and OC3" (IOP subset), N = 771. Overall RMSE for full NOMAD OC3 = 4.52, IOP subset OC3 = 14.8, IOP subset OC3" = 5.73. Overall mean normalized bias for full NOMAD OC3 = 19.1%, IOP subset OC3 = 19.3% and OC3" = 7.42%.

	Overall		443/547		489/547	
Method	Slope	y-int	Slope	y-int	Slope	y-int
OC3 (full NOMAD)	1.02 (*0.01*)	0.0199 (*0.0039*)	0.784 (*0.015*)	0.209 (*0.000*)	0.961 (*0.020*)	0.0615 (*0.0119*)
OC3 (IOP subset)	1.10 (*0.02*)	0.0286 (*0.0072*)	0.701 (*0.025*)	0.289 (*0.000*)	1.11 (*0.03*)	0.0545 (*0.0184*)
OC3" (IOP subset)	0.944 (*0.012*)	0.0175 (*0.005*)	0.862 (*0.021*)	0.0806 (*0.0000*)	0.804 (*0.032*)	0.103 (*0.025*)

While the errors in OC3 were unequal, the a_{dm}-free modeled data set showed uniform error across the dynamic range of [Chl] (Fig. 7). This suggests, as implied by the individual wavelength MBR regression coefficients, that OC3 might perform well on balance (overestimate ~underestimate), biases due to underlying variability in a_{ph}:a_{dm} and b_{bp} exist in the model. This absorption bias suggests that the distribution of satellite estimated

[Chl] is only comparable in a global sense where variability in a_{ph}:a_{dm} is averaged. Consequently, these biases also indicate that when moving between global to smaller regional and local scales, comparisons of [Chl] will be at a greater risk of error as the IOP relationships may be significantly different between two different regions or between the same region at a different time.

3.3 Radiative Transfer Model of Reflectance

The purpose of our Hydrolight modeling of computed reflectances was to provide a perspective on the expected, average global a_{ph}* and a measure of the sensitivity of empirical algorithms to changes in $\tilde{b}_{bp}$ which is linked to particle size [42]. By using a series of increasing [Chl] associated with defined a_{ph}* shapes provided by the model of Bricaud et al. [10] and two extreme $\tilde{b}_{bp}$ as input to Hydrolight, we bracketed the MBR variability between very small and large theoretical phytoplankton-like cell sizes (Fig. 8).

#163481 - $15.00 USD Received 22 Feb 2012; revised 11 Jul 2012; accepted 11 Jul 2012; published 29 Aug 2012

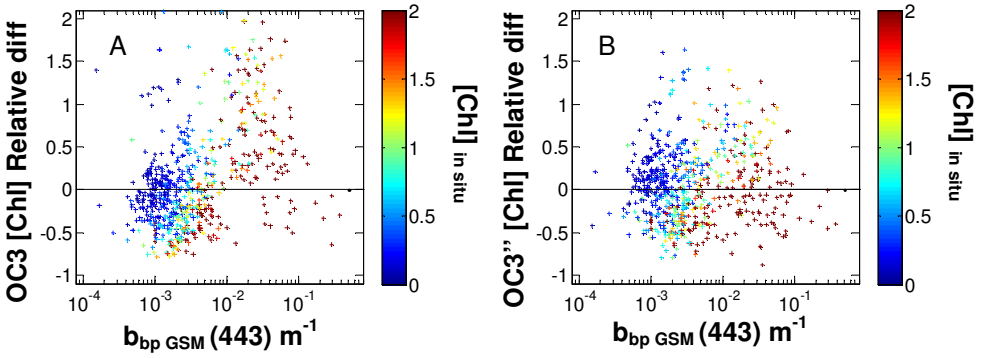

Fig. 7. [Chl] estimate error fields. Relative error in [Chl] from OC3 (A) and OC3" (B) vs. b_{bp} (443) and color coded by in situ [Chl]. OC3" had smaller, balanced relative errors while the error in OC3 was larger and biased.

The model demonstrates that variability in a_{ph}* determined the shape of OC3", moving smoothly along the gradient in the OC3" curve over a decreasing range of a_{ph}* at 444nm (0.050-0.022 m^2 mg/chl) specified by increasing [Chl] of ~0.5-5.0 mg chl/m^3. This suggests that a relatively narrow window of a_{ph}* spectral shapes was sufficient to match the average global [Chl] estimated by OC3". Considering the full distribution of MBRs in OC3", our Hydrolight model found that the OC3" data dispersion was bounded by only an order of magnitude in a_{ph}* (0.11-0.018 m^2 mg/chl at 444nm) specified by [Chl] from 0.05 to 10 mg chl/m^3.

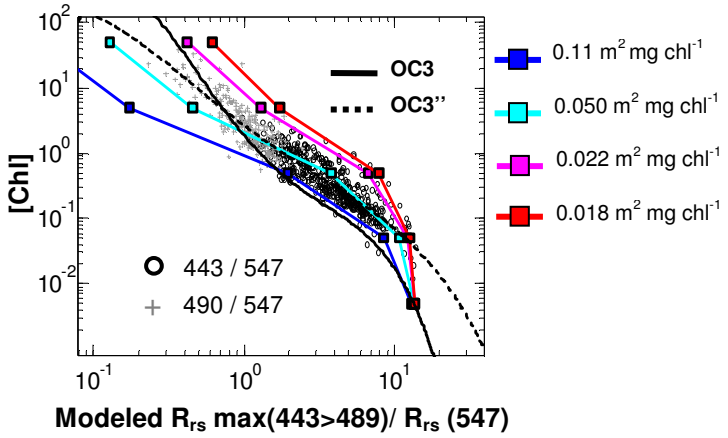

Fig. 8. Modeled in situ [Chl] vs. MBRs from Hydrolight a_{ph}-based modeled R_{rs} using high backscattering probability (Hydrolight Case 1 Large particle) relative to OC3" curve and data dispersion. OC3 provided for comparison. Colors specify 'OC3′ fits dependent on Chl-specific phytoplankton absorption (magnitude at 444nm shown to the side of plots). Data dispersion from in situ [Chl] vs. a_{dm}-free MBRs used to generate OC3" was bracketed by an order of magnitude range of Chl-specific phytoplankton absorption.

While the same a_{ph}* dependence would be expected to be found in OC3, it is well masked by the influence of a_{dm} variability on ocean color particularly for [Chl] below ~5 mg/m^3 (compare OC3 trend lines in Fig. 5). This is not surprising considering that a_{dm} variability exceeded a_{ph} variability relative to [Chl] in the NOMAD in situ data set (Fig. 2). In addition,

#163481 - $15.00 USD Received 22 Feb 2012; revised 11 Jul 2012; accepted 11 Jul 2012; published 29 Aug 2012

the masking of a_{ph}^* dependent modulation in OC3 agrees with the Brown et al. [22] assertion, based on a different NOMAD ocean color statistical approach, that chromophoric dissolved matter absorption (our a_{dm}) is the most important secondary influence on the shape of OC3.

In contrast to a_{ph}^* we found that our Hydrolight MBR model was relatively insensitive to $\tilde{b}_{bp}$ providing little impact on the shape of OC3" (data not shown). These results suggest that, despite the extreme range of size implied by b_{bp} spectral slope in the model, particle size would have a relatively minor influence on OC3. This implies that there is little opportunity to identify particle size class differences from ocean color through an MBR empirical methodology. Instead, the derivation of IOPs from remote-sensing reflectances first, should provide better insight into the biogeochemistry of dissolved and particulate matter in the ocean.

4. Conclusion

Our analyses of the NOMAD data set confirmed and quantified the sources of bias with regard to the IOPs that defined the NOMAD global training data set. Furthermore, unlike previous studies, we revealed the variability attributed to phytoplankton absorption in OC3 and the impact of a_{ph}^* and $\tilde{b}_{bp}$ variability on the structure of empirical algorithms. Phytoplankton and detrital absorption were similarly correlated in the NOMAD global ocean data set at 443 and 490nm, however, the variability in a_{dm} at both wavelengths relative to [Chl] in the global data set was approximately double that of a_{ph} indicating that ocean color variability in the NOMAD data set was dominated by a_{dm}.

The distribution of the ratio a_{ph}:a_{dm} in the NOMAD data subset indicated that the OC3 curve represents a best fit approach to encapsulate inherent (e.g., global) a_{ph} and a_{dm} in situ variability. But, while the best fit approach works reasonably well when considering the full dynamic range of MBR reflectances and [Chl], over smaller ranges (e.g., regional scales), the inherent IOP component variability limits the accuracy of MBR models to estimate [Chl]. At high MBRs and low [Chl], waters were weakly backscattering irrespective of whether absorption was dominated by a_{ph} or a_{dm}. In contrast to absorption, the distribution of b_{bp} magnitude remained similar in both OC3 and OC3" substantiating the covariation of b_{bp} with [Chl]. Expectedly, absorption component bias resulted in [Chl] underestimates of a_{ph} dominated samples and overestimates where a_{dm} dominated.

Our a_{dm}-free Hydrolight radiative transfer model covered a wide range of a_{ph}^* and bracketed a two order of magnitude variation in particle size revealing substantial modification in the shape of OC3". The variability in a_{dm}-free OC3" was found to be driven primarily by a relatively narrow order of magnitude window in a_{ph}^* with further minor variations due to changes in $\tilde{b}_{bp}$. While our model results indicated that shape modification of OC3" by both a_{ph}^* and $\tilde{b}_{bp}$ could potentially be used to identify changes in phytoplankton functional groups (see [25–27]), our study suggests that the influence of a_{dm} and b_{bp} on the shape of OC3 would most likely prohibit a statistical approach from identifying phytoplankton groups based on pigment characteristics and packaging.

Our study directly shows that IOP biases are contained within the foundation of ocean color data sets used to develop MBR-[Chl] algorithms. Empirical [Chl] estimates using these MBR algorithms whether on local, regional, or global spatial scales or for weekly, seasonal, or annual time-scales must assume that the mean IOP characteristics of their data set are similar to that of the IOP algorithm training set. This match in IOP component covariance allows for the most reduced set of remotely-sensed [Chl] estimate errors when considering a global scale of oceanic environments. However, consistent component absorption covariation is elusive in any of these cases exposing the weaknesses in empirical [Chl] algorithms. Extending satellite capabilities for ocean color biology requires recognizing the limitations of empirical algorithms to estimate [Chl] not only in complex coastal seas but also in global ocean settings. Due to natural IOP variability and the noncovariance observed on many spatial and temporal scales, the potential for large [Chl] uncertainties undermines the ability to

#163481 - $15.00 USD Received 22 Feb 2012; revised 11 Jul 2012; accepted 11 Jul 2012; published 29 Aug 2012

establish significant differences in historical [Chl] estimates on any scale below global trends. This demonstrates that the utilization of empirical methods could lead to substantial [Chl] estimate errors and the potential for implausible conclusions regarding long-term trends in phytoplankton productivity.

Moving towards understanding the sources of variability in absorption (as well as other inherent optical properties) and its influence on ocean color should be a primary focus. Semi-analytical algorithms that decompose the absorption signal into phytoplankton and detrital components represent an approach that allows for a direct relationship between [Chl] and phytoplankton absorption to be established. A reduction in error at local and regional levels for estimating biogeochemically important variables such as [Chl] is suggested as an outcome of this approach. Alternatively, establishing [Chl] estimate uncertainties for empirical algorithms based on the variability (dispersion) of [Chl] per reflectance ratio and uncertainties in sensor radiance measurements is vital to accurately portraying spatial and temporal differences in [Chl].

Acknowledgments

This work was funded by NASA Earth Space Fellowship #NNX08AU83H to MJS. The authors wish to thank three anonymous reviewers for their helpful comments and advice on this manuscript.

#163481 - $15.00 USD Received 22 Feb 2012; revised 11 Jul 2012; accepted 11 Jul 2012; published 29 Aug 2012